Catalysis Science & Technology

ROYAL SOCIETY OF CHEMISTRY

PAPER

View Article Online
View Journal | View Issue

Cite this: *Catal. Sci. Technol.*, 2022, 12, 3568

Fundamental understanding of the synthesis of well-defined supported non-noble metal intermetallic compound nanoparticles†

Yuanjun Song,[a] Yang He[b] and Siris Laursen *[c]

Access to well-defined, model-like, non-noble metal intermetallic compound nanomaterials (<10 nm) with phase pure bulk, bulk-like 1st-atomic-layer surface composition, and unique electronic and surface chemical properties is critical for the fields of catalysis, electronics, and sensor development. Non-noble metal intermetallic compounds are compositionally ordered solid compounds composed of transition metals and semimetals or post-transition metals. Their synthesis as model-like high-surface-area supported nanoparticles is challenging due to the elevated reactivity of the constituent elements and their interaction with the support material. In this study, we have developed a systematic understanding of the fundamental phenomena that control the synthesis of these materials such that phase pure bulk nanoparticles (<10 nm) may be produced with bulk-like surface terminations. The effects of the precursor and support choice, chemical potential of H_2, reduction temperature, and annealing procedures were investigated to understand the fundamental kinetics of particle formation and interactions that dictate phase purity and stability and 1st-atomic-layer surface composition. The understanding developed may serve as a foundation for further developing advanced synthesis procedures for well-defined nanoparticles with increasing compositional complexity.

Received 26th January 2022,
Accepted 8th April 2022

DOI: 10.1039/d2cy00183g

rsc.li/catalysis

1 Introduction

The science and technology of heterogeneous catalysis is particularly important in the 21st century due to pressing energy and environmental challenges that society faces. Catalytic materials play a central role in the production of nearly all fuels and chemicals and in the cleanup of the unwanted side products that pollute the environment.[1–6] For over a century, the field of catalysis has focused on the development of heterogeneous catalysts such as zeolites, platinum group metals (PGM), and PGM derived PGM + transition metal (TM) alloys.[7–16] These catalysts have exhibited sufficient, but not necessarily ideal catalytic performance in many foundational industrialized catalytic reactions. However, these classic catalytic materials often struggle to perform new reactions that require markedly different balances of surface chemistry. PGM-based catalysts are also very costly and limit widespread application of catalysis in distributed chemical and fuel production or use.[6,17–19] Therefore, the need for new, inexpensive non-noble metal-based catalytic materials that exhibit a much more diverse combination of surface chemistry towards C, O, and H and the bonds that contain them still persists. Of specific contemporary need are catalysts that exhibit elevated surface reactivity towards oxygen and nitrogen, lower surface reactivity towards unsaturated C=C bonds, limited hydrogenation kinetics, and activity in C–C, C–O, and C–N bond formation reactions.[15,18,20–35]

In the development of new heterogeneous catalysts, it is known that most pure elements outside of the noble metals exhibit too high chemical reactivity towards the organic elements (C, O, N, H, *etc.*) and bonds that contain them to be efficient catalysts at reasonable temperatures (T < 600 °C).[18,19,36] However, seminal ultra-high vacuum (UHV) surface science studies performed on single crystal materials clearly illustrated that the reactivity of non-noble metals (Mo, W, and V) could be reduced through the formation of TM solid compounds (Mo_2C, Mo_2N, VC, and W_2C) *via* reaction with p-block elements to produce surface chemistry similar

[a] *Joint International Research Laboratory of Information Display and Visualization, School of Electronic Science and Engineering, Southeast University, Nanjing, 210096, People's Republic of China*
[b] *Chemical Science Division, Oak Ridge National Laboratory, Oak Ridge, Tennessee 37831, USA*
[c] *Department of Chemical and Biomolecular Engineering, University of Tennessee, Knoxville, Tennessee 37996, USA. E-mail: slaursen@utk.edu; Fax: +1 865 9747076; Tel: +1 865 9745786*

† Electronic supplementary information (ESI) available: Additional EDX and XRD characterization, and a summary table of percentage of the NiGa phase after reduction with different H_2 chemical potentials. See DOI: https://doi.org/10.1039/d2cy00183g

to that of PGMs.[37–43] Further insight into potential new non-noble metal catalyst formulations was provided by studies that focused upon modification of existing noble (Pd, Pt, Rh, and Ru) and non-noble (Ni, Co, and Fe) metal catalysts with p-block elements (B, Al, Ge, Sn, Pb, Bi, Sb, Te, and Tl) to tune surface chemistry.[4,20,22,25,44–51] Later UHV surface science studies focused on the use of larger p-block elements in Pt_3-Sn, Pt_2Sn, PtSn, Pd_3Sn, and Pd_2Sn single crystals solidified the presence of unique surface chemistry presented by TM solid compounds.[4,22,47,52,53] These seminal studies illustrated that surface chemistry could be tuned to be more ideal in many catalytic reactions by the addition of p-block elements and have propelled the community to investigate TM solid compound catalysts. More recent studies have illustrated the utility of many TM solid compound catalysts in a host of classic and contemporary catalytic reactions with a notable focus on TM carbides and phosphides and TMs bound with post transition metals (Pd + Ga, Pd + In, Pd + Sn, Pt + Sn, Ni + Al, Ni + Ga, and Ni + Sn).[2,21,28,30,32,54–65] However, to systematically study and understand the surface chemistry and fully realize non-noble metal compound catalysts, the community needs high surface area materials that are well defined both in bulk crystal structure (phase) and surface composition. Herein, we focus on the fundamental aspects of the synthesis of well-defined/model-like supported high-surface-area binary non-noble TM solid compound nanoparticles composed of one TM element and one post-transition metal element. These atomically ordered TM solid compounds composed of crystalline mixtures of transition metals (TMs) and post-transition metals or semimetals (pTMs) are intermetallic compounds (IMCs), but are also known as ceramics in the materials science community and are distinct from compositionally disordered alloys.

Traditional methods for production of an ingot of material are through arc melting and high-frequency heating methods at high temperature, followed by ball-milling to produce particles with particle size on a scale of micrometers.[66–77] Despite the ingot method providing phase-pure materials initially, the method offers little control of morphology, particle size, and particle surface composition when producing particles from the ingot through grinding or ball milling.[66–68] In addition, the particles can be contaminated and oxidized during the milling process due to the use of a solvent. For example, Pd_2Ga synthesized by ball milling showed the formation of gallium oxide over the surface of the IM during ball milling.[78,79] This issue is often corrected by utilizing a reductive pre-treatment step after particle formation with and without additional annealing procedures. However, the initial oxidation can drive element segregation at the particle surface that may directly affect the particle surface composition even after reductive and annealing procedures.[58,80]

Low-temperature liquid phase methods such as co-reduction, sol–gel, solvothermal, and hydrothermal synthesis that produce IMC colloids have been developed and employ strong reducing agents to drive precursor reduction and IMC formation.[81–91] However, this approach can easily lead to kinetically trapped species and mixed-phase materials since the reducing agent cannot provide enough vibrational energy for structural relaxation of IMC crystallites. Likewise, highly reactive reducing and capping agents can strongly influence the particle surface composition and may drive the formation of surface compositions that include elements from the reagents when they are removed at elevated temperatures.

Supported IMC nanoparticles with a high surface area are generally much more favorable catalytic materials and have been prepared *via* incipient wetness impregnation, deposition precipitation, and chemical vapor deposition (CVD) methods.[3,5,23,54,59,67,92–97] However, many studies have produced multi-phase materials and have either not measured or used less-surface-sensitive techniques such as X-ray photoelectron spectroscopy (XPS) to measure IMC surface composition.[63,98–101] Nonetheless, some studies, including our investigations, have produced phase-pure materials to illustrate the effect of IMC composition on catalytic performance. For example, using the synthesis understanding presented herein, we prepared SiO_2 and Al_2O_3 supported Ni + Ga IMCs with a single pure bulk phase for dehydrogenation of alkane and propane steam reforming reactions.[28,30,32] Similarly, phase-pure Ni + Ga IMC catalysts have been illustrated in CO_2 partial reduction for the production of small alcohols.[3,5] Additionally, phase pure Ni_3Sn_2 nanoparticles on Al_2O_3, ZnO, and TiO_2 supports were shown to exhibit higher catalytic activity and improved selectivity in comparison to bulk Ni_3Sn_2 particles in the selective hydrogenation of unsaturated aldehydes for the production of unsaturated alcohols.[54] In addition, a suite of SiO_2 supported Ni + Sn IMCs with a pure bulk phase (Ni_3Sn, Ni_3Sn_2 and Ni_3Sn_4) were prepared by using the CVD method.[67] These studies illustrate that phase-pure supported IMC nanoparticle catalysts can be produced and the need for phase purity.

Beyond bulk phase purity, IMC particle surface composition must be similarly controlled and measured using appropriately surface sensitive techniques (*e.g.*, 1st atomic layer). Because of the general lack of truly surface sensitive characterization techniques, the dominant portion of prior studies has utilized techniques that yield information from the topmost several nanometers of the material (energy-dispersive X-ray spectroscopy (EDS) line scans and XPS) convoluting connections between surface composition and catalytic performance.[54,61,67,86,94,102–107] XPS has been employed routinely for many decades to study the elemental surface composition of solids and can be made to be more surface sensitive by tracking core electrons in the energy range of 50–250 eV, but still samples electrons from 1–5 nm into the material surface.[108–110] On the other hand, ablation or ion scattering methods, such time-of-flight secondary ion mass spectrometry (TOF-SIMS) and low or medium energy ion scattering (LEIS and MEIS), are more appropriate to yield more exact surface composition measurements.[111–116] Despite TOF-SIMS providing compositional information for

the first few atomic layers through the formation of free clusters produced by ablation/sputtering, the stability of the clusters can affect the suggested composition of the material surface.[114–117] On the other hand, ion scattering techniques allow for the measurement of the true 1st atomic layer surface composition. With a recent improvement in detector technology, the sensitivity of the LEIS technique has been dramatically improved and recoined as high-sensitivity LEIS (HS-LEIS) and is becoming more available to the community.[112,113,118–123] In the design of catalytic or sensing materials, it is vital to produce materials with measured and controlled 1st atomic layer compositions such that clear connections between surface composition and material performance may be developed.

Herein, we present many years of work that have focused upon understanding the critical fundamental aspects of the synthesis of well-defined/model-like high surface area supported nanoparticle late non-noble TM IMCs. Again, we define "well-defined/model-like" materials as materials that exhibit a single crystal phase and bulk-like surface compositions. This report outlines understanding developed through the synthesis of Ni + Ga, Ni + In, and Co + Ga IMCs. Our studies focused upon understanding the effects of precursor reduction kinetics, choice of inorganic precursor, H_2 chemical potential and temperature during reduction on the formation of the IMCs and the role of extended annealing environments in particle growth and particle surface composition. The effect of support surface chemistry on the formation of the IMCs was also investigated. These studies have shed light on the fundamental kinetics of precursor reduction, element diffusion across the support, and the formation of IMCs. It should be noted that the techniques developed in this study should enable the production of late TM IMCs when both TM and p-element precursors can be reduced at temperatures below 800 °C under pure H_2. Synthesis of IMCs composed of more reactive earlier TMs or p-elements will likely require higher energy techniques and/or organic precursors. Nonetheless, the understanding developed has paved the way for the community to access a large suite of model-like materials such that clear connections between surface chemistry and catalytic performance may be developed.

2 Method

2.1 Experimental method

2.1.1 Synthesis of supported intermetallic compounds. SiO_2 and partially oxidized carbon supported Ni + Ga IMC catalysts with 3 : 1, 5 : 3, 1 : 1, and 2 : 3 nominal loadings (10 wt%) were synthesized *via* the wet impregnation method. A defined amount of $Ni(NO_3)_2{\cdot}6H_2O$ (Sigma Aldrich) and $Ga(NO_3)_3{\cdot}xH_2O$ (Sigma Aldrich) metal precursors was deposited on SiO_2 (Alfa Aesar, amorphous fumed, 350–420 $m^2\ g^{-1}$)[124,125] or partially oxidized carbon. Partially oxidized carbon was homemade *via* oxidation of BLACK PEARLS® 2000 carbon black from CABOT corporation (1200–1500 $m^2\ g^{-1}$, 15 nm) in boiling 70% nitric acid solution with a reflux setup for 2 h, and the potential surface oxygen groups include CO- and CO_2-evolving carboxylic groups (such as C–OH, C–O–C, C═O and C–OOH).[126–128] $Ga(NO_3)_3$ was first dissolved in a small amount of 30 wt% nitric acid solution at 70 °C, then $Ni(NO_3)_2$ was added. After both precursors were completely dissolved, the mixture was deposited on the support. It is worth noting that inappropriate deposition procedures may produce inhomogeneous distributions of constituent elements on the support surface leading to multiphase IMCs.[129,130] Thus, the paste needs to be continually stirred for around 20 min till homogeneous and evaporative-transport of salts to evaporation fronts is limited. Then, all the samples were dried at 100 °C under Ar flow for 12 h.

Al_2O_3 (Alfa Aesar, 70% delta and 30% gamma, 50–100 nm)[28,30] supported 1 : 1 Ni : Ga IMCs (10 wt%) were synthesized *via* the hydroxide method using $Ni(NO_3)_2{\cdot}6H_2O$ (Sigma Aldrich) and $Ga(NO_3)_3{\cdot}xH_2O$ (Sigma Aldrich) metal precursors. A defined amount of $Ga(NO_3)_3{\cdot}xH_2O$ was first dissolved into 150 mL D.I. water at 70 °C. Then the pH value was adjusted to 3.9 using diluted NaOH solution to transform the Ga precursor into a hydroxy-nitrate. The support was then added to the solution and aged for 0.5 h. Next, a specific amount of $Ni(NO_3)_2{\cdot}6H_2O$ (1 : 1 Ni : Ga nominal loading) was introduced and transformed into the hydroxy-nitrate form at the pH of 7.0. The solution was aged for another 0.5 h. The sample was then washed, filtered, and then dried under air at 100 °C for 3 h. SiO_2 supported Ni + In (Ni_2In_3 and Ni_2In) IMCs were also synthesized using the same hydroxide method except for transforming $In(NO_3)_3{\cdot}xH_2O$ to hydroxy-nitrate species at pH = 3.

As-reduced samples were pretreated under pure H_2 at 700 °C for 2 h, and the effect of H_2 chemical potential (from 2% to 100%) and reduction temperature (400–700 °C) on the bulk composition, crystal phase distribution, and particle surface composition was investigated. Two types of annealing pretreatments including direct-annealing and freeze-annealing were performed. With direct-annealing, samples were annealed under 2% H_2 in Ar or pure Ar at 700 °C for 12 h directly after reduction without cooling treatment. On the other hand, freeze-annealing allowed particles to cool down to room temperature under H_2 to fully crystallize and then they were heated again to 700 °C under 2% H_2 for 12 h for annealing. Directly-annealed Ni_3Ga/SiO_2 was prepared *via* direct-annealing at 700 °C under 2% H_2 in Ar for 12 h directly after reduction of 3 : 1 Ni : Ga/SiO_2 under 100% H_2 at 700 °C for 2 h. Freeze-annealed samples were produced *via* freeze-annealing at 700 °C under 2% H_2 in Ar for 12 h after the reduction at 700 °C under 100% H_2 with cooling down to room temperature. To be clear, the temperature of the gas switch from 100% H_2 to 2% H_2 in direct-annealing was at 700 °C, while freeze-annealing was at room temperature.

2.1.2 Characterization. X-ray powder diffraction (XRD) on a PANalytical X'Pert Pro system using Cu Kα radiation (ORNL) was performed to identify the bulk phase and crystal

structure of particles. A long acquisition time of a minimum of 3 h was used to improve the detection of minority phases (the 2θ range is from 10 to 90° and the step size is 0.017° with a 0.006° s^{-1} scanning rate). To obtain more details of the crystal structure of the materials, high-resolution XRD with synchrotron radiation was performed at the beamline 11-BM at the Advanced Photon Source (APS) with mail-in service in Argonne National Laboratory, which uses an average wavelength of 0.41 with a step size of 0.001° and a scan speed of 0.01° s^{-1} and a 2θ range of 0.5–50°. With respect to the characterization of surface composition, high-sensitivity low energy ion scattering (HS-LEIS) spectroscopy with an IONTOF Qtac100 spectrometer (Lehigh University) was used. LEIS samples were prepared in our lab. After cooling down to room temperature, they were passivated under 2% O_2/Ar atmosphere for 1 hour which is the normal procedure used in the community to protect more reactive samples from autocatalytic oxidation. The samples were then transferred to a sealed sample tube filled with nitrogen. Before LEIS measurement, samples were introduced to the UHV chamber and exposed to room temperature low-energy neutral H atoms for 30 min to remove any oxidation layer. Both a surface survey scan and depth profiling were performed using 5 keV Ne^+ ions. In a surface survey scan, to seek targeted elements with a better signal-to-noise ratio, an ion dose of 5×10^{14} cm^{-2} with a wide energy range was used. In depth profiling, a sputter beam of 0.5 keV Ar^+ with 1×10^{14} ions per cm^2 was used for removal of approximately 0.1 nm atomic layer per cycle so that the ratio of integrated scattering intensity of probe elements (such as Ni-to-Ga) in each layer can be tracked and normalized to the bulk stoichiometry for the estimation of elemental composition at other layers. In this work, the depth profiling of SiO_2 supported Ni_3Ga and CoGa was performed to utilize them as the normalized references for the analysis of surface compositions of Ni + Ga and Co + Ga IMCs. Particle morphology, size, and size distribution were characterized utilizing transmission electron microscopy (TEM) and high-resolution energy-dispersive X-ray spectroscopy (HR-EDS). Samples were prepared by dispersing sample powder in methanol and sonicated before being deposited on the TEM grids. TEM measurements on all of the samples were performed on a ZEISS LIBRA 120 operating at 120 kV at the University of Tennessee, Knoxville. STEM HAADF and HR-EDS measurements were performed on a Talos FEI F200X operating at 200 kV at Oak Ridge National Lab (ORNL).

3 Results and discussion

3.1 Effect of salt choice on reduction dynamics

Studies first focused upon understanding the kinetics of inorganic precursor reduction using temperature-programmed reduction (TPR) by H_2 with the expectation that complete co-reduction of TM and p-element precursors was needed to promote the formation of phase pure IMC nanoparticles with stoichiometry that equalled that of

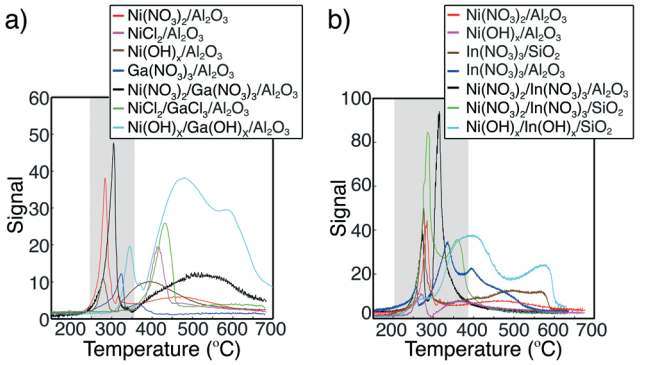

Fig. 1 Temperature programmed reduction (TPR) of Al_2O_3- and SiO_2-supported Ni, Ga, and In inorganic precursors (nitrate, chloride, or hydroxide) deposited alone or in binary couples (Ni + Ga or Ni + In). A weight loading of 10 wt% of each precursor was utilized. The reducing environment was 5% H_2 in Ar.

nominal loadings. The TPR of Ni, Ga, and In nitrate, chloride, and hydroxide precursor salts deposited on Al_2O_3 and SiO_2, alone and combined, was investigated in the context of forming Ni + Ga and Ni + In IMC nanoparticles (Fig. 1). In the individual TPR of the inorganic Ni and Ga nitrate, chloride, and hydroxide or In nitrate and hydroxide precursors, nitrate precursors exhibited more complete reduction at lower temperatures. The Ni and Ga chloride precursors required higher temperature for complete reduction and likely left chlorine at the metal–support interface.[131–134] All hydroxide precursors exhibited significant support-induced stabilization, which resulted in inhomogeneous reduction dynamics (bi- or multi-modal) and the need for higher temperatures for complete reduction.[135–137] The effect of support-induced stabilization and spillover of dissociated H_2 have been investigated and understood by many others previously in the synthesis of oxide-supported metal catalysts.[138–140] In co-deposition TPR studies, most of the same dynamics were observed, yet the presence of Ni helped to promote the reduction of p-element precursors likely *via* an atomic H spillover effect.[141,142] However, in the co-deposition of Ni and Ga or In hydroxides, support-induced stabilization resulted in even more pronounced inhomogeneous/multi-modal reduction dynamics. The effect of support choice, SiO_2 *vs.* Al_2O_3, was investigated for $In(NO_3)_3$ alone and co-deposited $Ni(NO_3)_2$ and $In(NO_3)_3$. Results indicated that $In(NO_3)_3$ was stabilized more over Al_2O_3 *vs.* SiO_2 resulting in more significant inhomogeneous reduction dynamics. However, when co-deposited with $Ni(NO_3)_2$, reduction was dramatically improved over both supports with complete reduction achieved below 450 °C. Results agree well with prior studies that investigated the TPR of various Ni inorganic salts.[132,143–145] In general, results indicated that nitrate salts would likely be most ideal to achieve complete reduction of both TM and p-element precursors at relatively low temperatures. Additionally, utilizing supports with low surface reactivity like SiO_2 can aid in ensuring complete

reduction of precursors. A similar conclusion was derived in a study focused on producing Pd-based IMCs with Bi, Sn, and Pb where $PdBi/Al_2O_3$ with a pure phase could be produced, yet Pd_3Sn and Pd_3Pb exhibited multi-phase compositions likely due to large differences in reduction kinetics of Pd, Sn, and Pb salts.[96]

It is useful to note that when extending these results to other precursors, one must be cognisant of and avoid the unfavorable formation of hydroxides or oxides during deposition when employing H_2O. For example, the $In(NO_3)_3$ precursor can react with H_2O to form complexes that contain hydroxide ligands that will stabilize the complex when in contact with certain supports and inhibit complete reduction.[146] One approach to avoid the formation of $In(OH)_x(NO_3)_x$ was to add a small amount of nitric acid to the slurry during deposition. In the synthesis of Ge-based IMCs, this issue is far more pronounced with GeO_2 formation occurring if aqueous deposition is attempted. Therefore, it may be necessary to utilize organometallic precursors in a water/air-free environment to produce IMCs from more reactive elements, *e.g.*, earlier TMs and later p-elements. For example, Komatsu and coworkers showed that phase pure Ni_3Ge could be produced inside the mesopores of MCM-41 through the formation of reduced Ni species followed by CVD of $Ge(CH_3)_4$ with H_2.[59] Likewise, the formation of phase pure IMCs of Mo, Ta, and Nb has only been achieved *via* the melt method or physical vapor deposition because of the stability of their inorganic salts and high oxophilicity leading to slow reduction kinetics.[71,73,74,147] In the end, production of IMCs composed of late-TMs and early and larger p-elements that are both easier to reduce when present as inorganic salts will likely be more facile. Meanwhile, production of IMCs composed of mid to early TMs or smaller or later p-elements may require new energy delivery techniques like light- or microwave-assisted reduction when using inorganic precursor salts or the use of organometallic precursors in water/air-free environments.

3.2 Effect of reduction temperature and support surface chemistry

After identifying precursors and conditions that allow for more complete reduction of precursors, we aimed to understand the effect of support surface chemistry on the formation of nanoparticle IMCs. We investigated the formation of Ni + Ga IMCs on fumed silica, partially oxidized carbon, and Al_2O_3 (70% delta, and 30% gamma) supports under 100% H_2 as a function of temperature. Ni + In IMC formation was only studied using the SiO_2 support. Nitrite precursors were deposited *via* wet impregnation and reduced using a minimum reduction temperature of 400 °C under 100% H_2 to ensure complete precursor reduction and limit any effects associated with limited H_2 chemical potential. Nominal loadings of 1 : 1 TM and p-elements were employed with the expectation that off-nominal TM-rich or lean stoichiometries could be produced if element diffusion or

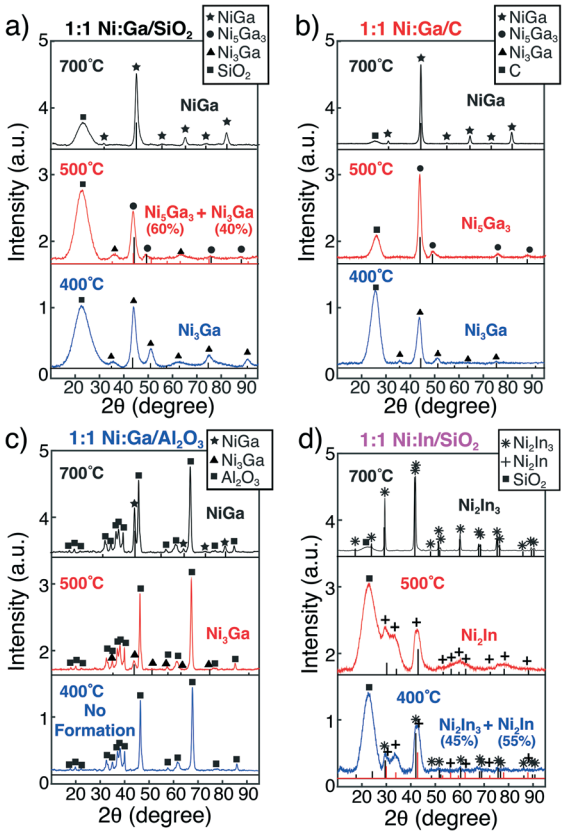

Fig. 2 Long-acquisition-time pXRD of a) 1 : 1 Ni : Ga/SiO_2, b) 1 : 1 Ni : Ga/C, c) 1 : 1 Ni : Ga/Al_2O_3, and d) 1 : 1 Ni : In/SiO_2 after reduction with pure H_2 at 400 °C, 500 °C, and 700 °C.

IMC kinetics were limited at the temperature employed. In the absence of kinetic limitations along the synthesis mechanism, production of the 1 : 1 phases of IMCs was expected, namely NiGa and NiIn. Long-acquisition time pXRD (3.5 h) was utilized to analyze the IMC phases produced (see Fig. 2a–d). The surface reactivity of the supports is expected to increase in the order of partially oxidized carbon < SiO_2 < Al_2O_3 and influence reduced element diffusion kinetics.

In the case of Ni + Ga IMC formation, a clear effect of support surface chemistry in dictating reduced element diffusion and IMC phase evolution was observed. The stability of the Ni + Ga IMC phases can be estimated from the phase diagram using melting points and is ordered from most to least stable as Ni_3Ga > Ni_5Ga_3 > NiGa.[148] The order of phase stability would also suggest the kinetics of formation of each phase if a BEP-like correlation between thermodynamics and kinetics exists. Indeed, Ni + Ga IMC synthesis using SiO_2 as a support illustrated that Ni_3Ga was the most kinetically preferred phase, as it formed readily in phase-pure form at 400 °C. As the reduction temperature increased to 500 °C, the next most stable phase of Ni_5Ga_3 dominated the sample with a minority of Ni_3Ga persisting. At 700 °C, the NiGa phase could be produced in pure form. These results suggested that the chemical potential of Ni and

Ga provided by the nominal loading was not sufficient to overcome kinetic limitations associated with reduced element diffusion at lower temperatures. However, it could dictate the IMC phase if appropriate vibrational energy was supplied. Utilizing a support with lower surface reactivity, namely partially oxidized carbon, the BEP-like correlation was still followed and phase pure Ni_3Ga could be produced at 400 °C, while pure phase Ni_5Ga_3 was produced at 500 °C and NiGa at 700 °C. Since the total metal loading was the same over SiO_2 *vs.* carbon supports, the width at half maximum of the pXRD reflections suggested that larger well-crystallized particles were produced over the carbon support further suggesting improved reduced element diffusion as support surface reactivity was reduced. Utilizing a support with elevated surface reactivity, namely Al_2O_3 (70% delta, and 30% gamma), significantly limited diffusion of the constituent elements inhibited the formation of Ni + Ga IMC at 400 °C. As the reduction temperature increased to 500 °C, the most kinetically preferred phase of Ni_3Ga was observed, which further confirms the effect of element availability on the IMC phase formed. At 700 °C, diffusion kinetics could be surmounted and the formation of NiGa could be achieved once again. Studies of Ni + In IMC formation over SiO_2 suggested that this phenomenon was general since a mixture of Ni_2In and Ni_2In_3 was produced at 400 °C, pure Ni_2In was produced at 500 °C, and Ni_2In_3 was produced at 700 °C, which agrees with the predicted stability of the Ni + In IMC phases in the studies of others.[60,149,150] A similar phenomenon was also encountered in the studies of Furukawa and Komatsu groups in the production of Pd_3Pb over SiO_2 and Al_2O_3 where phase pure Pd_3Pb could be achieved over SiO_2 and not over Al_2O_3 using the same reduction conditions (pure H_2 at 400 °C).[96,151] It is also useful to note that the strength of bonding between the constituent elements of the IMC and the support is species specific and the late TM elements will be less strongly bound than the more reactive p-elements. This phenomenon likely also dictates the IMC phases observed in this study and will become more prominent when more reactive constituent elements are employed. In the end, results suggested that utilizing supports with low surface reactivity towards the reduced elements of the IMC favorably promotes the formation of IMC phases that agree with nominal loadings. Therefore, support choice is critical in the production of well-defined supported IMC nanoparticles.

EDX elemental mapping in STEM of Ni + Ga IMC with 1 : 1 Ni : Ga nominal loading formation over and SiO_2 and Al_2O_3 (see Fig. 3) further confirmed the effect of temperature and support surface chemistry on element diffusion across the support surface. At a reduction temperature of 700 °C over SiO_2, the spatial distribution of Ni and Ga on SiO_2 indicated well-dispersed elements. The same phenomena were observed in the cases of Ni_3Ga/SiO_2 and Ni_5Ga_3/SiO_2 (see Fig. S1†). On the other hand, at 500 °C over Al_2O_3, Ni elements are observed to accumulate in particles, yet portions of the Ga loaded appear to remain dispersed across the support and not incorporated in the IMC particles formed. These results illustrate the difference in Ni *vs.* Ga diffusion and that Ga diffusion appears to limit the formation of an IMC phase that equals that of the nominal loading. As the p-element binds more strongly to the support, this trend is expected in the case of Ni-based IMCs.

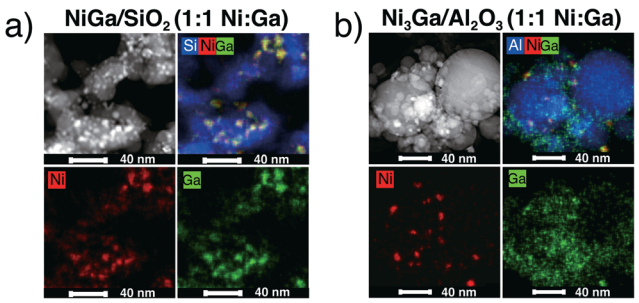

Fig. 3 EDX-mapping of a) NiGa (1 : 1 Ni : Ga nominal loading) over SiO_2, which was reduced at 700 °C with 100% H_2 for 2 h, and b) Ni_3Ga (1 : 1 Ni : Ga nominal loading) over Al_2O_3, which was reduced at 500 °C with 2% H_2 for 2 h, then annealed at 700 °C with pure Ar for 12 h. Element color code is: Ni (red), Ga (green), and Si or Al (blue).

3.3 Effect of H_2 chemical potential

To understand if there was an effect of H_2 chemical potential on element diffusion and IMC nanoparticle formation, we utilized Ni + Ga on fumed partially oxidized carbon, silica, and alumina supports deposited using nitrate salts at a loading of 1 : 1, reduced under at 700 °C in a range of H_2 concentrations (from 2% to 100%), and tracked the evolution of the IMC phases *via* p-XRD (Fig. 4). The percentage of the target IMC phase (NiGa) was summarized as a function of H_2 chemical potential in the ESI† (see Table S1). The reduction temperature of 700 °C was motivated by prior results that showed IMC phase formation that equaled nominal loading under 100% H_2. Gas phase flow conditions ensured that the availability of hydrogen was not limiting even at 2% H_2.

Results showed that the chemical potential of H_2 directly affected element diffusion and correlated well with the expected stability of reduced elements on the supports employed (partially oxidized carbon, SiO_2, and Al_2O_3) indicating a destabilizing effect of atomic H adatoms. Starting with the least reactive support, partially oxidized carbon, NiGa was achieved at a H_2 concentration of 5%, with a mixture of $Ni_{13}Ga_9$ and NiGa observed under 2% H_2. On the other hand, over SiO_2, 10% H_2 was needed to achieve pure NiGa, with mixtures of Ni_5Ga_3, $Ni_{13}Ga_9$, and NiGa observed at lower H_2 concentrations. Over the most reactive support utilized, Al_2O_3, an H_2 concentration of 50% was necessary to achieve phase pure NiGa. At lower H_2 concentrations, the IMC phases of Ni_5Ga_3 and Ni_3Ga were observed on Al_2O_3, sequentially. Observations suggest that atomic H adatoms either on the support or directly attached to the reduced constituent elements promote their diffusion across the surface of the support. If the H_2 chemical potential

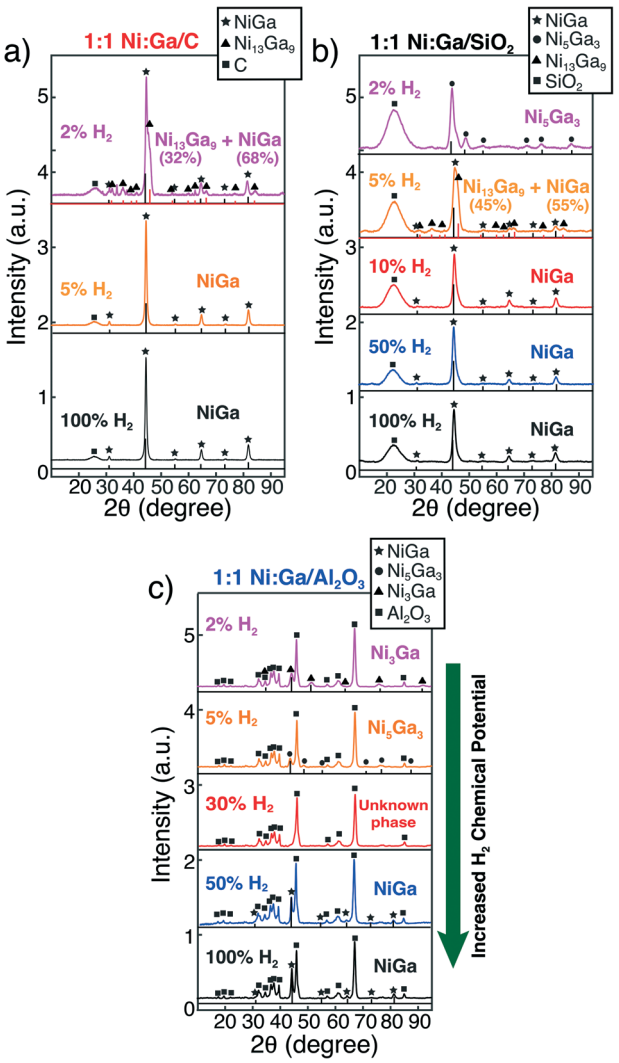

Fig. 4 Long-acquisition-time pXRD of a) 1 : 1 Ni : Ga/C, b) 1 : 1 Ni : Ga/SiO_2, and c) 1 : 1 Ni : Ga/Al_2O_3 after reduction with different concentrations of H_2 in Ar at 700 °C, which illustrated the effect of H_2 chemical potential on bulk composition.

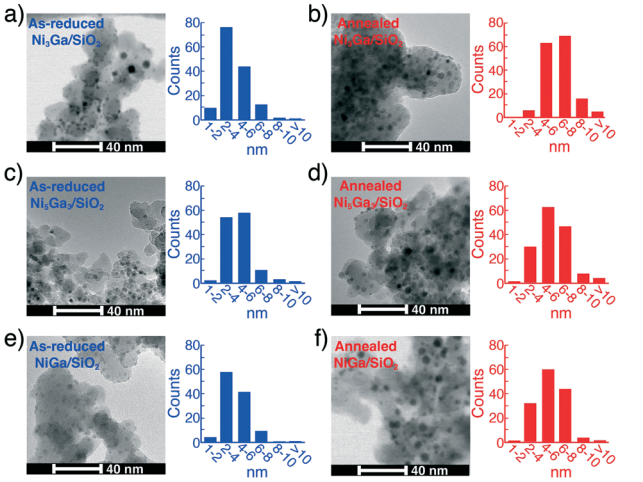

Fig. 5 Electron micrographs and size distributions of as-reduced and annealed SiO_2-supported Ni + Ga IMCs: a) as-reduced Ni_3Ga/SiO_2; b) directly-annealed Ni_3Ga/SiO_2; c) as-reduced Ni_5Ga_3/SiO_2; d) freeze-annealed Ni_5Ga_3/SiO_2; e) as-reduced NiGa/SiO_2; f) freeze-annealed NiGa/SiO_2. Minor particle size growth after 12 h at 700 °C illustrates the stability of the IMC nanoparticles.

is not sufficient, diffusion of constituent elements and their chemical potential with respect to IMC nanoparticle growth will be reduced. The effect is most pronounced again for the more reactive p-element, Ga, as evident by Ni-rich IMC compositions when diffusion is limited. The exact mechanism of the promotion of element diffusion cannot be derived from these studies, but it is reasonable to suggest that bonds between H and reduced elements weaken the bonds to the support surface and promote diffusion. It is less likely that the support surfaces become covered by H adatoms and limit the interaction between constituent elements and surface lattice elements. Further investigations are needed to fully understand the fundamental mechanism of this promotion. It is also reasonable to generalize these results and suggest that as constituent element reactivity increases, *e.g.*, early TMs or lighter p-elements, elevated chemical potentials of H_2 will be required to facilitate phase pure IMC nanoparticle formation. Utilizing supports with low surface reactivity would also be beneficial.

Using the understanding developed, we were able to synthesize suits of supported non-noble-metal IMC nanoparticles with a pure phase (as shown in Fig. S2†), including Ni + Ga (Ni_3Ga, Ni_5Ga_3, NiGa, Ni_2Ga_3), CoGa, and Ni + In IMCs (Ni_2In and Ni_2In_3). In addition, the particle size of the phase pure IMCs could be manipulated through an annealing pretreatment, as shown in Fig. 5. The IMC particle size of as-reduced IMCs was generally around 2–5 nm and could be increased to 4–8 nm after 12 h of annealing at 700 °C under Ar or 2% H_2 in Ar.

3.4 Fundamental setup for particle size growth and surface termination adjustment

Upon achieving phase pure IMC nanoparticle synthesis, we then focused upon developing annealing procedures to grow IMC particle size to improve bulk phase stability and to adjust particle surface composition to bulk-like where needed. The compositional and structural stabilities of IMCs are crucial if they are to be employed as catalysts, sensors, or electronic components that may encounter reactive gas phase environments at elevated temperatures or applied potentials. The performance of the supported IMC nanoparticles in catalytic, electronic, or sensing applications is affected by or directly dependent upon the compositional stability of the particle bulk,[19,21,152–155] surface composition,[64,80,156–159] and morphology of the particle.[91,160–162] Control of particle surface composition is also paramount in heterogeneous catalysis and sensing applications. Because the as-reduced Ni + Ga, CoGa, and Ni + In IMC nanoparticles exhibited average particle size distributions around 2–5 nm, their bulk and surface composition stability may be less than ideal for

applications that involve elevated temperatures ($T > 250$ °C) and contact with reactive chemical environments due to the nano-size effect. Moreover, the reactive environment used to form the IMC nanoparticles may result in element segregation to the particle surface.

Before discussing insights derived from developing annealing procedures, we review the observed IMC particle surface composition of the as-reduced IMCs synthesized. HS-LEIS was utilized to characterize IMC particle surface composition. HS-LEIS is a highly surface sensitive ion scattering technique that provides compositional information of the outermost 1st atomic layer of materials. The probe ion beam was rastered across the sample to minimize ion ablation effects, which are already fairly minimal and do not affect the dominant portion of ions that successfully scatter from the crystal surfaces.

HS-LEIS characterization of the as-reduced Ni_3Ga, Ni_5Ga_3, NiGa, CoGa, and Ni_2In_3 IMCs indicate that either the TM or the p-element could segregate to the particle surface under the preparation conditions (see Fig. 6). In the case of as-reduced Ni + Ga IMCs, Ni_3Ga exhibited a Ni-rich surface (92% Ni) while Ni_5Ga_3 and NiGa exhibited a surface composition close to that of the bulk (82% Ni and 46% Ni, respectively). On the other hand, as-reduced CoGa and Ni_2In_3 exhibited slightly Ga-rich (39% Co) and In-dominated (nearly 100% In) surface compositions. Results show that a rich energetic phase space determines the as-reduced IMC particle surface composition. For example, the more stable IMCs of Ni_3Ga, Ni_5Ga_3, NiGa, and CoGa promote TM-rich or near-bulk-like surface compositions. On the other hand, less stable IMCs composed of p-elements that present inordinately low pure-element surface energies, as in Ni_2In_3, resulted in p-element-dominated nanoparticle surface compositions. Comparing Ni_3Ga, Ni_5Ga_3, NiGa, and CoGa further suggested that the chemical potential of the elements within the IMC bulk, as dictated by the TM-to-p-element ratio, plays an energetically-similar role to the innate bulk IMC stability in determining IMC particle surface composition. This is evidenced by both NiGa and CoGa exhibiting more bulk-like surface terminations.

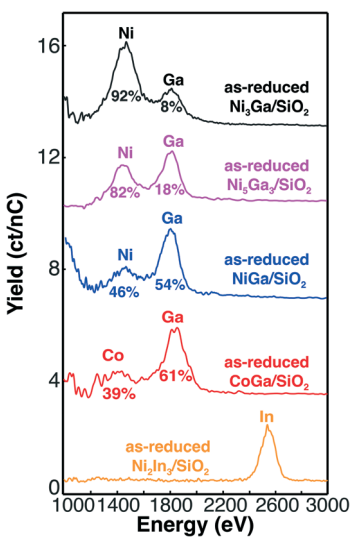

Fig. 6 First atomic layer surface composition characterization of as-reduced SiO_2 supported Ni_3Ga, Ni_5Ga_3, NiGa, CoGa, and Ni_2In_3 IMCs *via* HS-LEIS.

3.5 Effect of direct and freeze-annealing on phase disproportionation

Two annealing approaches were investigated to grow the particle size and adjust the particle surface composition: "direct-annealing" and "freeze-annealing". In direct-annealing, the as-reduced IMC was subjected to 12 h thermal treatment at the original 700 °C under a modified gas phase (2% H_2 in Ar or pure Ar) or under pure H_2 without intermediate cooling. In freeze-annealing, the as-reduced IMC was allowed to cool slowly to room temperature under H_2 then reheated to annealing conditions (700 °C for 12 h under 2% H_2 in Ar). A successful annealing procedure would result in the retention of the as-prepared IMC bulk crystal phase and a particle surface composition near that of the bulk stoichiometry. To clarify, annealing under 2% H_2 in Ar is different from a longer reduction treatment since the phase-pure IMC nanoparticles have already formed. In addition, as Fig. 4 illustrates, 2% H_2 in Ar is insufficient to promote the formation of the pure bulk phase that agrees with the nominal loading.

First focusing on the bulk crystal phase stability, we investigated the effect of direct-annealing samples under Ar at 700 °C for 12 h (see Fig. 7a). It was found that the procedure induced phase disproportionation of all the as-reduced Ni + Ga/SiO_2 IMCs. The bulk phases of Ni_3Ga/SiO_2, Ni_5Ga_3/SiO_2, and NiGa/SiO_2 disproportionated to a mixture of Ni_3Ga + Ni + NiO, Ni_3Ga, and a mixture of Ni_3Ga + Ga_2O_3, respectively (Fig. 7a). The source of oxygen for formation of NiO and Ga_2O_3 is likely from the SiO_2 support or the nitrates, which also has been observed in studies by other investigators.[163–166] When 2% H_2 in Ar was utilized during direct-annealing instead of pure Ar, disproportionation in Ni_3Ga was avoided, yet still occurred for the less stable phases of Ni_5Ga_3 and NiGa (Fig. 7b). When utilizing pure H_2 during direct-annealing, phase disproportionation was avoided in all the Ni + Ga IMC cases (Fig. 7c). Phase disproportionation driven by direct-annealing treatment was also found to be support-dependent and that supports with lower surface reactivity would limit constituent element spill over and phase disproportionation. For example, when utilizing a support with lower surface reactivity, *e.g.*, partially oxidized carbon, the phase purity of NiGa could be retained after direct-annealing under pure Ar and 2% H_2 in Ar (see Fig. 7d).

These results suggested that the stability of the IMC nanoparticles directly after their formation at 700 °C was dependent upon the presence of atomic H adsorbates. It is proposed that strong interactions between constituent

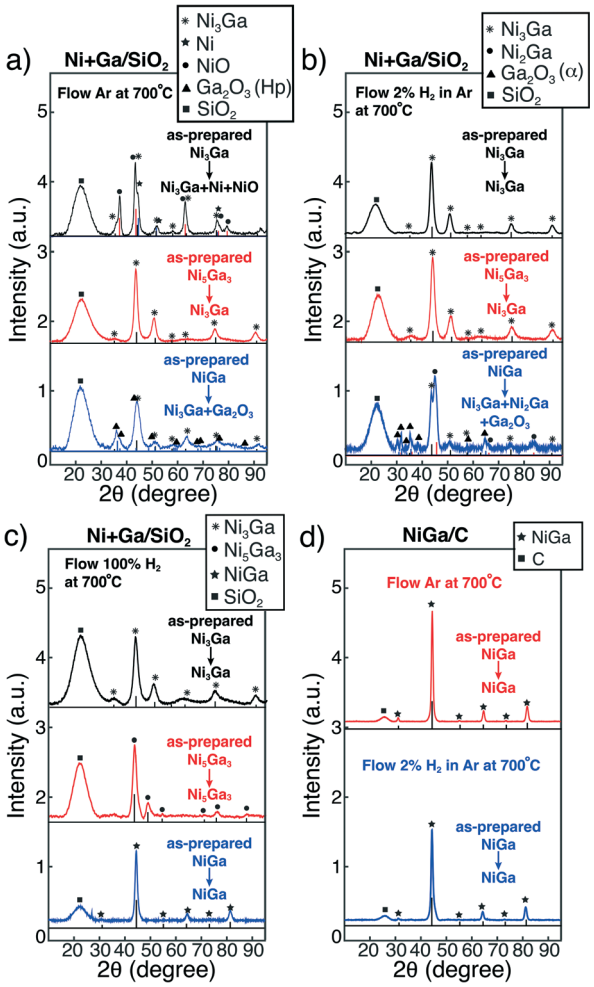

Fig. 7 The effect of direct-annealing as a function of the gas phase H_2 concentration and support on IMC initial phase stability: a) as-prepared Ni + Ga/SiO_2 at 700 °C under pure Ar; b) as-prepared Ni + Ga/SiO_2 at 700 °C under 2% H_2 in Ar; c) as-prepared Ni + Ga/SiO_2 at 700 °C under 100% H_2; and d) as-prepared NiGa/C at 700 °C under pure Ar and 2% H_2 in Ar.

elements and the support surface may drive a spill-over-like effect that drives constituent elements back onto the support promoting disproportionation when atomic H adsorbates were absent. In the presence of atomic H adsorbates, elements that spill over onto the support may be destabilized *via* the same mechanism observed in the initial reductive treatment to form the IMCs. This mechanism appears to promote constituent elements to remain in the IMC particle. Despite this favorable effect, using high H_2 chemical potentials during annealing may lead to element segregation to the IMC particle surfaces because of strong H-element interaction. Therefore, alternate annealing procedures that avoid or minimize the need for H_2 in the gas phase were investigated.

The freeze-annealing procedure was developed through systematic investigation of the effect of direct-annealing temperature on phase disproportionation of SiO_2 supported as-reduced NiGa IMCs and revealed that allowing particles to

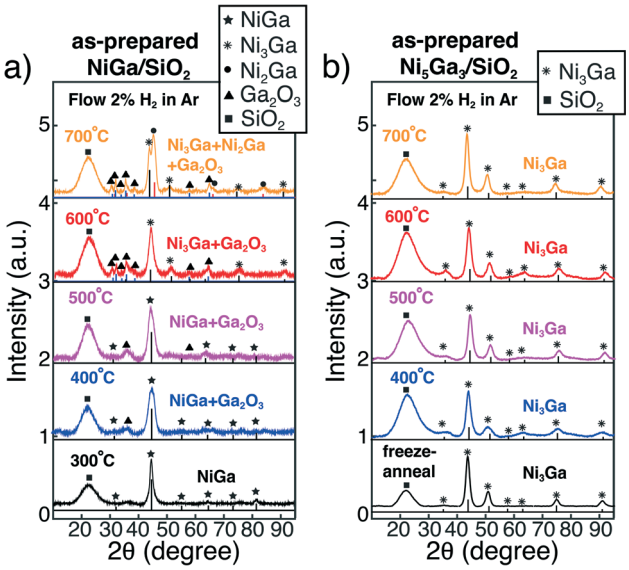

Fig. 8 Effect of direct-annealing temperature on IMC phase stability: a) direct-annealing of as-prepared NiGa/SiO_2 at 300–700 °C under 2% H_2 in Ar; b) direct-annealing of as-prepared Ni_5Ga_3/SiO_2 at 400–700 °C and freeze-annealing at 700 °C under 2% H_2 in Ar.

fully crystallize by cooling samples to room temperature under H_2 after initial reduction could aid in avoiding phase disproportionation. As shown in Fig. 8a, with direct-annealing at 700 °C, SiO_2-supported NiGa was completely transformed to a mixture of Ni_3Ga, Ni_2Ga, and Ga_2O_3 as a result of the spill-over effect. Similarly, at 600 °C, NiGa transformed to a mixture of Ni_3Ga and Ga_2O_3. However, when the direct-annealing temperature decreased to 500 °C and 400 °C, the NiGa phase could be maintained but still coexisted with Ga_2O_3. Once the temperature was reduced to 300 °C, pure NiGa could be retained.

Shifting to allow the as-prepared IMCs to cool to room temperature under H_2 to allow them to fully crystallize before increasing the temperature back up to 700 °C for annealing allowed a lower concentration of 2% H_2 to be utilized during annealing. Using this approach, IMC particles of Ni_3Ga, NiGa, CoGa, and Ni_2In_3 remained phase pure after freeze-annealing and enabled the growth of IMC particle sizes from 2–5 nm to 4–8 nm (see Fig. 9 and 5). In the case of Ni_5Ga_3, disproportionation was observed even using the freeze-annealing procedure using 2% H_2 in Ar (see Fig. 8b). These results indicate that the relative stability of the IMC and support surface chemistry towards the constituent elements play a role in IMC stability under annealing conditions and that atomic H adsorbates can counteract spillover effects that lead to phase disproportionation.

3.6 Annealing to adjust particle surface composition

Returning to focus upon IMC particle surface composition, the direct- and freeze-annealing procedures developed were able to adjust the particle surface composition to bulk-like in the cases of Ni_3Ga, NiGa, and CoGa while retaining the initial

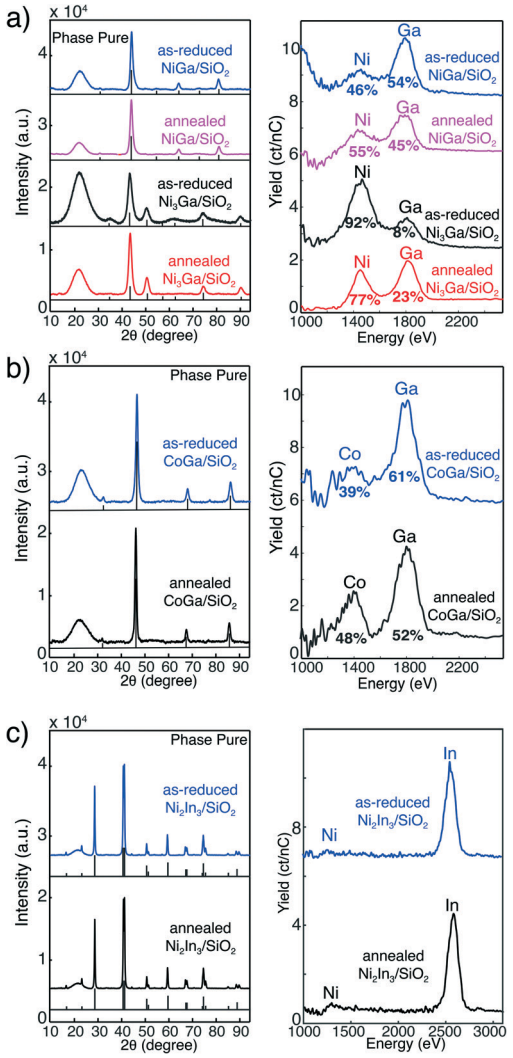

Fig. 9 Demonstration of well-defined IMCs with phase pure bulk and controllable particle surface composition. Long-acquisition-time pXRD and HS-LEIS characterization of: a) as-reduced and freeze-annealed $NiGa/SiO_2$, and as-reduced and directly-annealed Ni_3Ga/SiO_2; b) as-reduced and freeze-annealed $CoGa/SiO_2$; and c) as-reduced and freeze-annealed Ni_2In_3/SiO_2.

phase purity of the IMCs (see Fig. 9a and b). This phenomenon was previously encountered by others in studies where bulk phases of Pt + Ga were maintained under annealing pretreatment and control of surface termination was achieved *via* annealing at different temperatures in spite of using less surface sensitive XPS.[167,168] Ni_2In_3 was the only case where annealing procedures could grow the particle size and retain the initial phase purity, but not adjust the In-rich surface composition back to bulk-like (see Fig. 9c). Fundamentally, results further underscore that the innate stability and relative chemical potential of constituent elements as dictated by the bulk composition and nano-size effects that destabilize bonding compete with surface energy as a function of surface composition to dictate particle surface composition. Despite the seemingly minor increase in particle size from 2–5 nm to 4–8 nm after 12 h of annealing at 700 °C, results suggest that the IMCs are significantly stabilized, which may also help energetically drive an adjustment to bulk-like surface composition. Prior catalytic studies also illustrated the increase in Ni + Ga IMC nanoparticle stability after annealing, as evidenced by phase purity being retained even after experiencing gas phase reaction conditions of direct ethane and propane dehydrogenation and propane wet reforming up to 600 °C with a very minor particle size increase after 35 to 82 h.[28,30,32]

In the case of less stable IMC compositions that contain elements that exhibit markedly low surface energy in pure form, *e.g.*, Ni_2In_3, the freeze-annealing conditions used clearly cannot readjust IMC particle surface composition and alternate etching or preparation approaches may be required.[16,68,169] These results agree with calculated surface energies of a pure In surface *vs.* a bulk-like terminated $Ni_2In_3(110)$ surface where the former is lower in energy.[169]

Another possible approach to control IMC particle surface composition would be to utilize specific gas phase environments that contain specific molecules that bind more strongly to one of the constituent elements of the IMC.[156] For example, utilizing an olefin or CO in combination with H_2 during the initial reduction or annealing procedure may selectively promote higher concentrations of the TM element at the IMC particle surface. This approach was successful for Arenz and co-workers in the manipulation of the surface composition of Pt_3Co where a mixed $PtCo_x$ surface composition could be modified to Pt-rich by using CO during annealing procedures.[156,170] Likewise, the study of Fe–Cr alloys by Park and co-workers indicated that increased H_2 concentration of the annealing atmosphere modified the surfaces from Fe-rich to Cr-rich due to the more significant H–Cr interaction.[170] Summarizing, we were able to achieve particle growth and bulk-like surface composition of a selection of IMCs using a freeze-annealing procedure that employed low concentrations of H_2 ultimately achieving well-defined model-like materials.

4 Conclusion

This study developed a fundamental understanding of the synthesis of well-defined supported IMC nanoparticles with a pure bulk phase and controllable surface compositions. The understanding can be applied to the entire field of synthesis of well-defined IMCs and enable fundamental structure–activity correlation studies in the fields of heterogeneous catalysis, sensing, and electronics. The fundamental phenomena determined to dictate the formation of well-defined supported IMC nanoparticles were: i) reduction kinetics of inorganic salt precursors, ii) formation kinetics of IMCs as a function of the diffusion of constituent elements on the surface, iii) the role of support surface chemistry, iv) innate IMC phase stability, and v) the effect of H_2 chemical potential of the reducing and annealing environment. The understanding developed herein can be applied and extended to the entire TM + p-element IMC compositional space with

the understanding that the availability of reduced constituent elements and their diffusion across the support will be significant factors when using earlier TMs or more reactive p-elements. Careful choice of precursors and supports with low reactivity will be necessary to realize the synthesis of the entire IMC compositional space as supported nanoparticles.

Conflicts of interest

There are no conflicts to declare.

Acknowledgements

This research was supported by the National Science Foundation (NSF) CAREER award (Grant CBET-1752063) and the American Chemical Society Petroleum Research Fund (Grant PRF# 57589-ND5). Regular XRD analysis was conducted at the Center for Nanophase Materials Sciences (CNMS project number CNMS2018-374) at Oak Ridge National Lab (ORNL). This work utilized the Advanced Photon Source for HR-XRD analysis at Argonne National Laboratory supported by the U. S. Department of Energy, Office of Science, Office of Basic Energy Sciences, under Contract No. DE-AC02-06CH11357.

Notes and references

1 C. Breinlich, J. Haubrich, C. Becker, A. Valcarcel, F. Delbecq and K. Wandelt, *J. Catal.*, 2007, **251**, 123–130.
2 A. Onda, T. Komatsu and T. Yashima, *Phys. Chem. Chem. Phys.*, 2000, **2**, 2999–3005.
3 F. Studt, I. Sharafutdinov, F. Abild-Pedersen, C. F. Elkjær, J. S. Hummelshoj, S. Dahl, I. Chorkendorff and J. K. Norskov, *Nat. Chem.*, 2014, **6**, 320–324.
4 H. Zhao and B. E. Koel, *Surf. Sci.*, 2004, **572**, 261–268.
5 I. Sharafutdinov, C. F. Elkjær, H. W. Pereira de Carvalho, D. Gardini, G. L. Chiarello, C. D. Damsgaard, J. B. Wagner, J.-D. Grunwaldt, S. Dahl and I. Chorkendorff, *J. Catal.*, 2014, **320**, 77–88.
6 L. Zhang, L. Xue, B. Lin, Q. Zhao, S. Wan, Y. Wang, H. Jia and H. Xiong, *ChemSusChem*, 2022, **15**, e202102494.
7 J. Zhang, L. Wang, Y. Shao, Y. Wang, B. C. Gates and F. Xiao, *Angew. Chem., Int. Ed.*, 2017, **56**, 9747–9751.
8 N. Tahsini, A.-C. Yang, V. Streibel, B. Werghi, E. D. Goodman, A. Aitbekova, S. R. Bare, Y. Li, F. Abild-Pedersen and M. Cargnello, *J. Am. Chem. Soc.*, 2022, **144**, 1612–1621.
9 S. W. Chee, J. M. Arce-Ramos, W. Li, A. Genest and U. Mirsaidov, *Nat. Commun.*, 2020, **11**, 2133.
10 M. A. van Spronsen, J. W. M. Frenken and I. M. N. Groot, *Chem. Soc. Rev.*, 2017, **46**, 4347–4374.
11 J. Gustafson, O. Balmes, C. Zhang, M. Shipilin, A. Schaefer, B. Hagman, L. R. Merte, N. M. Martin, P.-A. Carlsson, M. Jankowski, E. J. Crumlin and E. Lundgren, *ACS Catal.*, 2018, **8**, 4438–4445.
12 X. Su, P. S. Cremer, Y. R. Shen and G. A. Somorjai, *J. Am. Chem. Soc.*, 1997, **119**, 3994–4000.
13 T.-H. Yang, J. Ahn, S. Shi, P. Wang, R. Gao and D. Qin, *Chem. Rev.*, 2020, **121**, 796–833.
14 A. Borgschulte, R. Westerwaal, J. Rector, H. Schreuders, B. Dam and R. Griessen, *J. Catal.*, 2006, **239**, 263–271.
15 L. E. Murillo, C. A. Menning and J. G. Chen, *J. Catal.*, 2009, **268**, 335–342.
16 H.-Y. Park, T.-Y. Jeon, J. H. Jang, S. J. Yoo, K.-H. Choi, N. Jung, Y.-H. Chung, M. Ahn, Y.-H. Cho and K.-S. Lee, *et al.*, *Appl. Catal., A*, 2013, **129**, 375–381.
17 A. Bruix, Y. Lykhach, I. Matolínová, A. Neitzel, T. Skála, N. Tsud, M. Vorokhta, V. Stetsovych, K. Ševčíková, J. Mysliveček, R. Fiala, M. Václavů, K. C. Prince, S. Bruyère, V. Potin, F. Illas, V. Matolín, J. Libuda and K. M. Neyman, *Angew. Chem., Int. Ed.*, 2014, **53**, 10525–10530.
18 F. Studt, F. Abild-Pedersen, T. Bligaard, R. Z. Sorensen, C. H. Christensen and J. K. Norskov, *Science*, 2008, **320**, 1320–1322.
19 L. Rößner and M. Armbrüster, *ACS Catal.*, 2019, **9**, 2018–2062.
20 E. W. Shin, C. H. Choi, K. S. Chang, Y. H. Na and S. H. Moon, *Catal. Today*, 1998, **44**, 137–143.
21 M. Armbrüster, K. Kovnir, M. Behrens, D. Teschner, Y. Grin and R. Schlögl, *J. Am. Chem. Soc.*, 2010, **132**, 14745–14747.
22 H. Zhao, J. Kim and B. E. Koel, *Surf. Sci.*, 2003, **538**, 147–159.
23 B. Riguetto, C. Rodrigues, M. Morales, E. Baggio-Saitovitch, L. Gengembre, E. Payen, C. Marques and J. Bueno, *Appl. Catal., A*, 2007, **318**, 70–78.
24 H. Göksu, S. F. Ho, Ö. Metin, K. Korkmaz, A. Mendoza Garcia, M. S. Gültekin and S. Sun, *ACS Catal.*, 2014, **4**, 1777–1782.
25 K. Tomishige, K. Asakura and Y. Iwasawa, *J. Catal.*, 1994, **149**, 70–80.
26 Y. He and S. Laursen, *ACS Catal.*, 2017, **7**, 3169–3180.
27 Y. He and S. Laursen, *Catal. Sci. Technol.*, 2018, **8**, 5302–5314.
28 Y. He, Y. Song, D. A. Cullen and S. Laursen, *J. Am. Chem. Soc.*, 2018, **140**, 14010–14014.
29 Y. He and S. Laursen, *Surf. Sci.*, 2019, **686**, 1–9.
30 Y. He, Y. Song and S. Laursen, *ACS Catal.*, 2019, **9**, 10464–10468.
31 Y. Song and S. Laursen, *J. Catal.*, 2019, **372**, 151–162.
32 Y. Song, Y. He and S. Laursen, *ACS Catal.*, 2020, **10**, 8968–8980.
33 S. Poudyal and S. Laursen, *J. Phys. Chem. C*, 2018, **122**, 8045–8057.
34 S. Poudyal and S. Laursen, *Catal. Sci. Technol.*, 2019, **9**, 1048–1059.
35 S. Poudyal, M. Parker and S. Laursen, *J. Phys. Chem. Lett.*, 2019, **10**, 4603–4608.
36 J. K. Nørskov, F. Abild-Pedersen, F. Studt and T. Bligaard, *Proc. Natl. Acad. Sci. U. S. A.*, 2011, **108**, 937–943.
37 J. Chen, *J. Catal.*, 1995, **154**, 80–90.
38 J. G. Chen, M. D. Weisel, Z. M. Liu and J. M. White, *J. Am. Chem. Soc.*, 1993, **115**, 8875–8876.

39 H. Ren, Y. Chen, Y. Huang, W. Deng, D. G. Vlachos and J. G. Chen, *Green Chem.*, 2014, **16**, 761–769.
40 J. Chen and B. Fruhberger, *Surf. Sci.*, 1996, **367**, L102–L110.
41 B. M. Wyvratt, J. R. Gaudet, D. B. Pardue, A. Marton, S. Rudić, E. A. Mader, T. R. Cundari, J. M. Mayer and L. T. Thompson, *ACS Catal.*, 2016, **6**, 5797–5806.
42 M. Neylon, S. Choi, H. Kwon, K. Curry and L. Thompson, *Appl. Catal., A*, 1999, **183**, 253–263.
43 M. D. Porosoff, S. Kattel, W. Li, P. Liu and J. G. Chen, *Chem. Commun.*, 2015, **51**, 6988–6991.
44 J. Giner, *J. Catal.*, 1967, **9**, 115–124.
45 S. Kishida, *J. Catal.*, 1968, **12**, 97–101.
46 M. Masai, *J. Catal.*, 1975, **38**, 128–134.
47 C. Xu and B. E. Koel, *Surf. Sci.*, 1994, **304**, 249–266.
48 P. Forzatti, *J. Catal.*, 1982, **76**, 188–207.
49 Y. Nitta, T. Imanaka and S. Teranishi, *Bull. Chem. Soc. Jpn.*, 1981, **54**, 3579–3580.
50 J. A. Schreifels, P. C. Maybury and W. E. Swartz, *J. Org. Chem.*, 1981, **46**, 1263–1269.
51 H. Aduriz, *J. Catal.*, 1989, **119**, 97–107.
52 G. Hamm, T. Schmidt, J. Breitbach, D. Franke, C. Becker and K. Wandelt, *Surf. Sci.*, 2004, **562**, 170–182.
53 D. I. Jerdev, A. Olivas and B. E. Koel, *J. Catal.*, 2002, **205**, 278–288.
54 R. Rodiansono, M. D. Astuti, S. Khairi and S. Shimazu, *Bull. Chem. React. Eng. Catal.*, 2016, **11**, 1.
55 C. Li, Y. Chen, S. Zhang, J. Zhou, F. Wang, S. He, M. Wei, D. Evans and X. Duan, *ChemCatChem*, 2014, **6**, 824–831.
56 J. Gao, H. Zhao, X. Yang, B. E. Koel and S. G. Podkolzin, *ACS Catal.*, 2013, **3**, 1149–1153.
57 Q. Feng, S. Zhao, Y. Wang, J. Dong, W. Chen, D. He, D. Wang, J. Yang, Y. Zhu and H. Zhu, *et al.*, *J. Am. Chem. Soc.*, 2017, **139**, 7294–7301.
58 K. Kovnir, J. Osswald, M. Armbruster, D. Teschner, G. W. U. Wild, A. Knop-Gericke, T. Ressler, Y. Grin and R. Schlogl, *J. Catal.*, 2009, **264**, 93–103.
59 T. Komatsu, T. Kishi and T. Gorai, *J. Catal.*, 2008, **259**, 174–182.
60 Y. Chen and J. Chen, *Appl. Surf. Sci.*, 2016, **387**, 16–27.
61 J. Shabaker, D. Simonetti, R. Cortright and J. Dumesic, *J. Catal.*, 2005, **231**, 67–76.
62 A. García-Trenco, A. Regoutz, E. R. White, D. J. Payne, M. S. Shaffer and C. K. Williams, *Appl. Catal., B*, 2018, **220**, 9–18.
63 T. Komatsu, M. Mesuda and T. Yashima, *Appl. Catal., A*, 2000, **194–195**, 333–339.
64 S. Penner and P. D. Kheyrollahi Nezhad, *ACS Catal.*, 2021, **11**, 5271–5286.
65 L. Xiao, P. Hu, Z.-J. Sui, D. Chen, X.-G. Zhou, W.-K. Yuan and Y.-A. Zhu, *J. Catal.*, 2021, **404**, 32–45.
66 M. G. Kanatzidis, R. Pöttgen and W. Jeitschko, *Angew. Chem., Int. Ed.*, 2005, **44**, 6996–7023.
67 A. Onda, T. Komatsu and T. Yashima, *J. Catal.*, 2004, **221**, 378–385.
68 J. Osswald, R. Giedigkeit, R. Jentoft, M. Armbruster, F. Girgsdies, K. Kovnir, T. Ressler, Y. Grin and R. Schlogl, *J. Catal.*, 2008, **258**, 210–218.
69 M. Fan, Y. Xu, J. Sakurai, M. Demura, T. Hirano, Y. Teraoka and A. Yoshigoe, *Int. J. Hydrogen Energy*, 2015, **40**, 12663–12673.
70 C. Yeh and C. Yeh, *J. Alloys Compd.*, 2005, **388**, 241–249.
71 C. Milanese, F. Maglia, A. Tacca, U. Anselmi-Tamburini, C. Zanotti and P. Giuliani, *J. Alloys Compd.*, 2006, **421**, 156–162.
72 S. Meschel, P. Nash and X.-Q. Chen, *J. Alloys Compd.*, 2010, **492**, 105–115.
73 V. Gauthier, F. Bernard, E. Gaffet, D. Vrel, M. Gailhanou and J. Larpin, *Intermetallics*, 2002, **10**, 377–389.
74 H. Yoshida, T. Shima, T. Takahashi and H. Fujimori, *Mater. Trans., JIM*, 1999, **40**, 455–458.
75 T. Chanadee, J. Wannasin and S. Niyomwas, *J. Ceram. Soc. Jpn.*, 2014, **122**, 496–501.
76 L. A. Arkatova, L. N. Kurina and L. V. Galaktionova, *Russ. J. Phys. Chem. A*, 2009, **83**, 624–629.
77 N. Köwitsch, S. Barth, K. Ploner, R. Blume, D. Teschner, S. Penner and M. Armbrüster, *ChemPhysChem*, 2022, **23**, e202200074.
78 G. Wowsnick, D. Teschner, M. Armbrüster, I. Kasatkin, F. Girgsdies, Y. Grin, R. Schlögl and M. Behrens, *J. Catal.*, 2014, **309**, 221–230.
79 G. Wowsnick, D. Teschner, I. Kasatkin, F. Girgsdies, M. Armbrüster, A. Zhang, Y. Grin, R. Schlögl and M. Behrens, *J. Catal.*, 2014, **309**, 209–220.
80 S. Zafeiratos, S. Piccinin and D. Teschner, *Catal. Sci. Technol.*, 2012, **2**, 1787.
81 L. Zhen, Y. X. Gong, J. T. Jiang and W. Z. Shao, *J. Appl. Phys.*, 2008, **104**, 034312.
82 Z. Cui, H. Chen, M. Zhao and F. J. DiSalvo, *Nano Lett.*, 2016, **16**, 2560–2566.
83 Y.-T. Pan, Y. Yan, Y.-T. Shao, J.-M. Zuo and H. Yang, *Nano Lett.*, 2016, **16**, 6599–6603.
84 J.-H. Liu, L.-D. Meng, C.-Q. Lv and G.-C. Wang, *RSC Adv.*, 2016, **6**, 14593–14601.
85 J. C. Bauer, X. Chen, Q. Liu, T.-H. Phan and R. E. Schaak, *J. Mater. Chem.*, 2008, **18**, 275–282.
86 X. Chen, M. Li, J. Guan, X. Wang, C. T. Williams and C. Liang, *Ind. Eng. Chem. Res.*, 2012, **51**, 3604–3611.
87 R. E. Cable and R. E. Schaak, *Chem. Mater.*, 2007, **19**, 4098–4104.
88 R. E. Cable and R. E. Schaak, *Chem. Mater.*, 2005, **17**, 6835–6841.
89 A. K. Sra and R. E. Schaak, *J. Am. Chem. Soc.*, 2004, **126**, 6667–6672.
90 R. E. Schaak, A. K. Sra, B. M. Leonard, R. E. Cable, J. C. Bauer, Y.-F. Han, J. Means, W. Teizer, Y. Vasquez and E. S. Funck, *J. Am. Chem. Soc.*, 2005, **127**, 3506–3515.
91 Y. Yuan, Z. Yang, W. Lai, L. Gao, M. Li, J. Zhang and H. Huang, *Chem. – Eur. J.*, 2021, **27**, 16564–16580.
92 S. Furukawa, K. Takahashi and T. Komatsu, *Chem. Sci.*, 2016, **7**, 4476–4484.
93 L. Sordelli, R. Psaro, G. Vlaic, A. Cepparo, S. Recchia, C. Dossi, A. Fusi and R. Zanoni, *J. Catal.*, 1999, **182**, 186–198.
94 C. Li, Y. Chen, S. Zhang, S. Xu, J. Zhou, F. Wang, M. Wei, D. G. Evans and X. Duan, *Chem. Mater.*, 2013, **25**, 3888–3896.

95 J. L. Snider, V. Streibel, M. A. Hubert, T. S. Choksi, E. Valle, D. C. Upham, J. Schumann, M. S. Duyar, A. Gallo, F. Abild-Pedersen and T. F. Jaramillo, *ACS Catal.*, 2019, **9**, 3399–3412.
96 S. Furukawa, K. Ozawa and T. Komatsu, *RSC Adv.*, 2013, **3**, 23269.
97 L. Li, B. Zhang, E. Kunkes, K. Föttinger, M. Armbrüster, D. S. Su, W. Wei, R. Schlögl and M. Behrens, *ChemCatChem*, 2012, **4**, 1764–1775.
98 J. Serrano-Ruiz, A. Sepúlveda-Escribano, F. Rodríguez-Reinoso and D. Duprez, *J. Mol. Catal. A: Chem.*, 2007, **268**, 227–234.
99 F. Marchesini, S. Irusta, C. Querini and E. Miró, *Appl. Catal., A*, 2008, **348**, 60–70.
100 J. Llorca, *J. Catal.*, 1995, **156**, 139–146.
101 N. Kaylor, J. Xie, Y.-S. Kim, H. N. Pham, A. K. Datye, Y.-K. Lee and R. J. Davis, *J. Catal.*, 2016, **344**, 202–212.
102 J. Zhou, Y. Yang, C. Li, S. Zhang, Y. Chen, S. Shi and M. Wei, *J. Mater. Chem. A*, 2016, **4**, 12825–12832.
103 J. Shabaker, G. Huber and J. Dumesic, *J. Catal.*, 2004, **222**, 180–191.
104 C. Rudolf, B. Dragoi, A. Ungureanu, A. Chirieac, S. Royer, A. Nastro and E. Dumitriu, *Catal. Sci. Technol.*, 2014, **4**, 179–189.
105 Y. Ma, Y. Xu, M. Demura, D. H. Chun, G. Xie and T. Hirano, *Catal. Lett.*, 2006, **112**, 31–36.
106 X. Chen, Y. Ma, L. Wang, Z. Yang, S. Jin, L. Zhang and C. Liang, *ChemCatChem*, 2015, **7**, 978–983.
107 T. Komatsu, M. Fukui and T. Yashima, *Stud. Surf. Sci. Catal.*, 1996, 1095–1104.
108 V. Lockett, R. Sedev, C. Bassell and J. Ralston, *Phys. Chem. Chem. Phys.*, 2008, **10**, 1330.
109 R. Steinberger, C. Celedón, B. Bruckner, D. Roth, J. Duchoslav, M. Arndt, P. Kürnsteiner, T. Steck, J. Faderl and C. Riener, *et al.*, *Appl. Surf. Sci.*, 2017, **411**, 189–196.
110 K. Cai, M. Müller, J. Bossert, A. Rechtenbach and K. D. Jandt, *Appl. Surf. Sci.*, 2005, **250**, 252–267.
111 J. Zheng, J. Qu, H. Lin, Q. Zhang, X. Yuan, Y. Yang and Y. Yuan, *ACS Catal.*, 2016, **6**, 6662–6669.
112 F. Polo-Garzon, S.-Z. Yang, V. Fung, G. S. Foo, E. E. Bickel, M. F. Chisholm, D.-e. Jiang and Z. Wu, *Angew. Chem., Int. Ed.*, 2017, **56**, 9820–9824.
113 G. S. Foo, Z. D. Hood and Z. Wu, *ACS Catal.*, 2017, **8**, 555–565.
114 M. Lefèvre, J. P. Dodelet and P. Bertrand, *J. Phys. Chem. B*, 2005, **109**, 16718–16724.
115 R. N. S. Sodhi, *Analyst*, 2004, **129**, 483–487.
116 D. J. Graham and D. G. Castner, *Biointerphases*, 2012, **7**, 49.
117 P. Massonnet and R. M. A. Heeren, *J. Anal. At. Spectrom.*, 2019, **34**, 2217–2228.
118 S. P. Phivilay, C. A. Roberts, A. A. Puretzky, K. Domen and I. E. Wachs, *J. Phys. Chem. Lett.*, 2013, **4**, 3719–3724.
119 S. P. Phivilay, C. A. Roberts, A. D. Gamalski, E. A. Stach, S. Zhang, L. Nguyen, Y. Tang, A. Xiong, A. A. Puretzky and F. F. Tao, *et al.*, *ACS Catal.*, 2018, **8**, 6650–6658.
120 G. S. Foo, F. Polo-Garzon, V. Fung, D.-e. Jiang, S. H. Overbury and Z. Wu, *ACS Catal.*, 2017, **7**, 4423–4434.
121 G. M. Rupp, H. Téllez, J. Druce, A. Limbeck, T. Ishihara, J. Kilner and J. Fleig, *J. Mater. Chem. A*, 2015, **3**, 22759–22769.
122 X. Li, D. Li, H. Tian, L. Zeng, Z.-J. Zhao and J. Gong, *Appl. Catal., B*, 2017, **202**, 683–694.
123 J. Druce, H. Téllez, M. Burriel, M. D. Sharp, L. J. Fawcett, S. N. Cook, D. S. McPhail, T. Ishihara, H. H. Brongersma and J. A. Kilner, *Energy Environ. Sci.*, 2014, **7**, 3593–3599.
124 X. Li, W. Ji, J. Zhao, S. Wang and C. Au, *J. Catal.*, 2005, **236**, 181–189.
125 L. Wang, Y. Yi, Y. Zhao, R. Zhang, J. Zhang and H. Guo, *ACS Catal.*, 2015, **5**, 4167–4174.
126 Z. Lu, G. Chen, S. Siahrostami, Z. Chen, K. Liu, J. Xie, L. Liao, T. Wu, D. Lin, Y. Liu, T. F. Jaramillo, J. K. Nørskov and Y. Cui, *Nat. Catal.*, 2018, **1**, 156–162.
127 J. H. Kim, J. Y. Cheon, T. J. Shin, J. Y. Park and S. H. Joo, *Carbon*, 2016, **101**, 449–457.
128 D. J. Suh, P. Tae-Jin and I. Son-Ki, *Carbon*, 1993, **31**, 427–435.
129 E. Plessers, J. E. vandenReijen, P. E. deJongh, K. P. deJong and M. B. J. Roeffaers, *ChemCatChem*, 2017, **9**, 4562–4569.
130 W. Juszczyk, Z. Karpinski, D. Lomot, J. Pielaszek, Z. Paal and A. Stakheev, *J. Catal.*, 1993, **142**, 617–629.
131 S. Wang and G. Lu, *Appl. Catal., A*, 1998, **169**, 271–280.
132 E. Kowalewski, I. I. Kamińska, G. Słowik, D. Lisovytskiy and A. Śrębowata, *React. Kinet., Mech. Catal.*, 2017, **121**, 3–16.
133 S. Laursen and S. Linic, *J. Phys. Chem. C*, 2009, **113**, 6689–6693.
134 S. Laursen and S. Linic, *Phys. Chem. Chem. Phys.*, 2009, **11**, 11006.
135 X. Wen, R. Li, Y. Yang, J. Chen and F. Zhang, *Appl. Catal., A*, 2013, **468**, 204–215.
136 Y. Huang, X. Chen, Y. Deng, D. Zhou and L. Wang, *Chem. Eng. J.*, 2015, **269**, 434–443.
137 M. A. Ermakova and D. Y. Ermakov, *Appl. Catal., A*, 2003, **245**, 277–288.
138 E. v. Steen, G. S. Sewell, R. A. Makhothe, C. Micklethwaite, H. Manstein, M. de Lange and C. T. O'Connor, *J. Catal.*, 1996, **162**, 220–229.
139 H. Kusaka, Y. Hara, M. Onuki, T. Akai and M. Okuda, *J. Catal.*, 1996, **161**, 96–106.
140 D. Eliche-Quesada, J. Mérida-Robles, E. Rodríguez-Castellón and A. Jiménez-López, *Appl. Catal., A*, 2005, **279**, 209–221.
141 W. C. Conner and J. L. Falconer, *Chem. Rev.*, 1995, **95**, 759–788.
142 B. Sen, *J. Catal.*, 1989, **117**, 404–415.
143 P. Kim, H. Kim, J. B. Joo, W. Kim, I. K. Song and J. Yi, *J. Mol. Catal. A: Chem.*, 2006, **256**, 178–183.
144 G. Wu, C. Zhang, S. Li, Z. Han, T. Wang, X. Ma and J. Gong, *ACS Sustainable Chem. Eng.*, 2013, **1**, 1052–1062.
145 N. Keghouche, S. Chettibi, F. Latrèche, M. Bettahar, J. Belloni and J. Marignier, *Radiat. Phys. Chem.*, 2005, **74**, 185–200.
146 W. W. Rudolph, D. Fischer, M. R. Tomney and C. C. Pye, *Phys. Chem. Chem. Phys.*, 2004, **6**, 5145–5155.
147 F. Maglia, U. Anselmi-Tamburini, N. Bertolino, C. Milanese and Z. A. Munir, *J. Mater. Res.*, 2001, **16**, 534–544.

148 H. Okamoto, *J. Phase Equilib. Diffus.*, 2008, **29**, 296–296.
149 P. Durussel, G. Burri and P. Feschotte, *J. Alloys Compd.*, 1997, **257**, 253–258.
150 L. Wang, X. Niu and J. Chen, *Appl. Catal., B*, 2020, **278**, 119293.
151 T. Komatsu, *Appl. Catal., A*, 2003, **251**, 315–326.
152 A. P. Tsai, S. Kameoka, K. Nozawa, M. Shimoda and Y. Ishii, *Acc. Chem. Res.*, 2017, **50**, 2879–2885.
153 A. K. Vivekanandan, B. Muthukutty, S.-M. Chen, M. Sivakumar and S.-H. Chen, *ACS Sustainable Chem. Eng.*, 2020, **8**, 17718–17726.
154 Y. Satake, K. Fujiwara, J. Shiogai, T. Seki and A. Tsukazaki, *Sci. Rep.*, 2019, **9**, 3282.
155 Z. Fang, S. Duan, H. Liu, Z. Hong, H. Wu, F. Zhao, Q. Li, S. Fan, W. Duan and J. Wang, *Small*, 2021, **18**, 2105172.
156 K. Mayrhofer, V. Juhart, K. Hartl, M. Hanzlik and M. Arenz, *Angew. Chem., Int. Ed.*, 2009, **48**, 3529–3531.
157 M. Friedrich, D. Teschner, A. Knop-Gericke and M. Armbrüster, *J. Catal.*, 2012, **285**, 41–47.
158 B. Zugic, L. Wang, C. Heine, D. N. Zakharov, B. A. J. Lechner, E. A. Stach, J. Biener, M. Salmeron, R. J. Madix and C. M. Friend, *Nat. Mater.*, 2016, **16**, 558–564.
159 M. Krajčí and J. Hafner, *Phys. Rev. B: Condens. Matter Mater. Phys.*, 2013, **87**, 035436.
160 E. Antolini, *Appl. Catal., B*, 2017, **217**, 201–213.
161 S. Furukawa and T. Komatsu, *ACS Catal.*, 2016, **7**, 735–765.
162 P. Dantzer, *Mater. Sci. Eng., A*, 2002, **329–331**, 313–320.
163 H. Orita, *J. Catal.*, 1984, **90**, 183–193.
164 C. C. Tang, S. S. Fan, H. Y. Dang, P. Li and Y. M. Liu, *Appl. Phys. Lett.*, 2000, **77**, 1961–1963.
165 P. Burattin, M. Che and C. Louis, *J. Phys. Chem. B*, 1999, **103**, 6171–6178.
166 W. Jóźwiak, M. Nowosielska and J. Rynkowski, *Appl. Catal., A*, 2005, **280**, 233–244.
167 Y. K. Kim, D. A. Baugh, D. K. Shuh, R. Stanley Williams, L. P. Sadwick and K. L. Wang, *J. Mater. Res.*, 1990, **5**, 2139–2151.
168 D. Rosenthal, R. Widmer, R. Wagner, P. Gille, M. Armbrüster, Y. Grin, R. Schlögl and O. Gröning, *Langmuir*, 2012, **28**, 6848–6856.
169 L. Vitos, A. Ruban, H. Skriver and J. Kollár, *Surf. Sci.*, 1998, **411**, 186–202.
170 E. Park, B. Hüning and M. Spiegel, *Appl. Surf. Sci.*, 2005, **249**, 127–138.